Protecting Spin Coherence in a Tunable Heisenberg Model

Emily J. Davis,[1] Avikar Periwal,[1] Eric S. Cooper,[1] Gregory Bentsen,[1,2] Simon J. Evered,[1] Katherine Van Kirk,[1] and Monika H. Schleier-Smith[1,3]

[1]*Department of Physics, Stanford University, Stanford, California 94305, USA*
[2]*Department of Physics, Princeton University, Princeton, New Jersey 08540, USA*
[3]*SLAC National Accelerator Laboratory, Menlo Park, California 94025, USA*

(Received 12 March 2020; revised 15 May 2020; accepted 9 June 2020; published 3 August 2020)

Using an ensemble of atoms in an optical cavity, we engineer a family of nonlocal Heisenberg Hamiltonians with continuously tunable anisotropy of the spin-spin couplings. We thus gain access to a rich phase diagram, including a paramagnetic-to-ferromagnetic Ising phase transition that manifests as a diverging magnetic susceptibility at the critical point. The susceptibility displays a symmetry between Ising interactions and XY (spin-exchange) interactions of the opposite sign, which is indicative of the spatially extended atomic system behaving as a single collective spin. Images of the magnetization dynamics show that spin-exchange interactions protect the coherence of the collective spin, even against inhomogeneous fields that completely dephase the noninteracting and Ising systems. Our results underscore prospects for harnessing spin-exchange interactions to enhance the robustness of spin squeezing protocols.

DOI: 10.1103/PhysRevLett.125.060402

Models of quantum magnetism capture the physics of diverse systems ranging from ferromagnets to resonating valence bond solids [1] and quantum spin liquids [2]. Implementing such models using cold atoms or molecules [3–10] opens pathways both for elucidating the physics of materials and for accessing new quantum many-body phenomena [11–25]. Several prospects, including simulating spin glasses [15–17] or information scrambling in black holes [18–20], require exotic nonlocal interactions. Nonlocal spin-spin couplings can also aid in combinatorial optimization [26,27], investigating new forms of integrability [22] or nonequilibrium phase transitions [28–30], and preparing entangled states [31–38].

Nonlocal spin models are naturally realized in cavity-QED experiments, where the cavity mediates interactions among distant atoms [30–34,39–44]. For atoms coupled to a single cavity mode, the dynamics are often approximated by viewing the system as a single collective spin [45–47]. In practice, spatial inhomogeneities interfere with this approximation. For studies of many-body physics, inhomogeneities facilitate access to a larger Hilbert space compared with that of a spatially uniform system [20,22]. In the context of quantum state engineering, however, inhomogeneities adversely impact metrological protocols that benefit from maximizing spin coherence [32,46–48].

A demonstrated approach to protecting spin coherence is to harness suitably designed interactions [49–52]. Examples include collisional spin self-rephasing in Bose-Einstein condensates [49,50] and temporal ordering in disordered dipolar materials [51]. In the cavity-QED context, spin-exchange interactions [40,42] have been proposed as a mechanism for preventing dephasing during spin squeezing protocols [37], by providing an energy gap between manifolds of different total spin [40]. While Ref. [40] has shown spectroscopic evidence of this energy gap, an observation of enhanced spin coherence—or a comparison with Ising interactions employed for squeezing to date [31–33]—has hitherto been lacking.

Here, we report on realizing and probing a family of tunable nonlocal Heisenberg models for spins encoded in Zeeman states of atoms in an optical cavity (Fig. 1). The strengths and signs of spin-exchange (XY) and Ising couplings mediated by the cavity are fully controlled by magnetic and optical fields. We demonstrate this tunability by Hamiltonian tomography and by probing the magnetic susceptibility. The susceptibility reveals a paramagnetic-to-ferromagnetic phase transition arising in both the *ferromagnetic* Ising and *antiferromagnetic* XY models. Yet comparing effects of Ising and spin-exchange interactions on spin coherence reveals a striking difference, with XY interactions protecting against inhomogeneous fields that otherwise completely dephase the system.

The interactions that we engineer are described by a Hamiltonian [22]:

$$H_{XXZ}/\hbar = J^{xy}(\Theta)[\mathcal{F}_x^2 + \mathcal{F}_y^2] + J^z(\Theta)\mathcal{F}_z^2. \qquad (1)$$

Here, $\boldsymbol{\mathcal{F}} \equiv \sum_i c_i \mathbf{f}_i$ is a weighted collective spin vector that accounts for nonuniform couplings to the cavity mode, parametrized by c_i for atom i with spin $\mathbf{f}_i$. The weights c_i are normalized such that they average to one. The relative strength of the spin-exchange coupling J^{xy} and Ising coupling J^z is governed by the angle Θ between the cavity

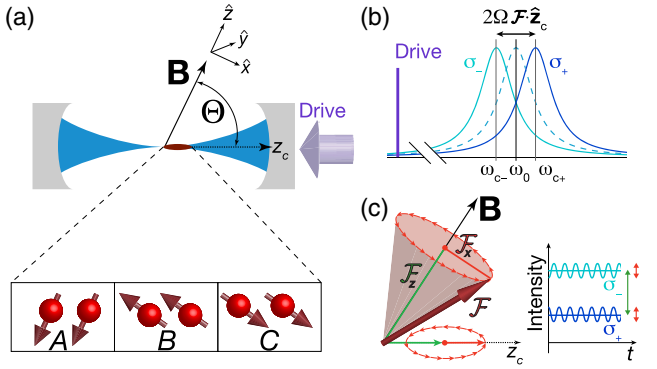

FIG. 1. Experimental scheme for engineering Heisenberg interactions. (a) Atomic spins in optical cavity precess about magnetic field $\mathbf{B}$ at angle Θ from cavity axis $\hat{\mathbf{z}}_c$. The enlargement shows spin texture with three distinct regions A, B, C as starting point for Hamiltonian tomography. (b) Atom-induced birefringent splitting $\omega_{c+} - \omega_{c-} = 2\Omega\boldsymbol{\mathcal{F}} \cdot \hat{\mathbf{z}}_c$ of $\sigma_\pm$ cavity modes. (c) Effect of precessing spins on intracavity intensities of $\sigma_\pm$ light: projection of static z component (green) shifts dc level to generate Ising interactions, while oscillating projections of transverse components (red) modulate the intensities to generate spin-exchange interactions.

axis and an external magnetic field $\mathbf{B}$, which defines the quantization axis $\hat{\mathbf{z}} = \mathbf{B}/B$ for the spins [Fig. 1(a)]. We view the system in a frame rotating about $\mathbf{B}$ at the Larmor frequency (Zeeman splitting) $\omega_Z = \mu_B B/2$.

The underlying mechanism for the tunable interactions is the Faraday effect [53]: the atomic magnetization generates circular birefringence for the intracavity light, which acts back on the atoms via a vector light shift. Specifically, the magnetization component along the cavity axis $\hat{\mathbf{z}}_c$ couples to the light, introducing a birefringent splitting $\omega_{c+} - \omega_{c-} = 2\Omega\boldsymbol{\mathcal{F}} \cdot \hat{\mathbf{z}}_c$ between the frequencies of the $\sigma_\pm$ cavity modes [Fig. 1(b)], where Ω parametrizes the average birefringence per atom. Driving the cavity with linearly polarized light of frequency ω_d injects σ_+ and σ_- photons into the cavity. For large drive detuning $\delta = \omega_d - \omega_0$ from cavity resonance, the birefringence unbalances the $\sigma_\pm$ intracavity intensities [Fig. 1(c)], producing a vector light shift.

Ising interactions arise when the applied magnetic field $\mathbf{B}$ is oriented along the cavity axis, i.e., $\hat{\mathbf{z}} = \hat{\mathbf{z}}_c$. The Faraday effect then yields a vector light shift $\propto \mathcal{F}_z$, producing the $\mathcal{F}_z^2$ terms in the Hamiltonian, akin to Refs. [31–33]. XY interactions arise when $\mathbf{B}$ has a component orthogonal to the cavity axis [42]. In the lab frame, the transverse spin components (x, y) then have oscillating projections along the cavity axis that modulate the polarization of the intracavity light at the Larmor frequency ω_Z [Fig. 1(c)]. This polarization modulation acts as a rotating transverse field that drives spin flips.... Provided that the drive is detuned from resonance for Raman processes that flip a single spin [54], the lowest-order resonant process is pairwise spin exchange [42].

Our experiments employ the $f = 1$ hyperfine spins of ^{87}Rb atoms, which interact via a near-concentric optical cavity (Fig. 1). A cloud of $N = 1 \times 10^5$ laser-cooled atoms is trapped in a 1560-nm intracavity lattice. The cloud length is comparable to the Rayleigh range $z_R = 1.4$ mm of the cavity. Interactions are mediated by a 780-nm TEM_{00} mode of linewidth $\kappa = 2\pi \times 200$ kHz, detuned by $\Delta = -2\pi \times 11$ GHz from the $|5S_{1/2}, f = 1\rangle \rightarrow |5P_{3/2}\rangle$ transition. The vacuum Rabi frequency $2g = 2\pi \times 2.5$ MHz on the cycling transition produces a maximal vector light shift $\Omega_0 = -g^2/6\Delta = 2\pi \times 23$ Hz per circularly polarized intracavity photon, for a cold atom at an antinode at cavity center. This value is reduced to $\Omega = 2\pi \times 7(1)$ Hz for an average atom due to the rms transverse cloud size of 13 μm and to displacement from cavity center [55].

We benchmark our implementation of the tunable Heisenberg Hamiltonian [Eq. (1)] by extracting the Ising and XY couplings $J^{z,xy}$ from quench dynamics. We design initial states such that J^z or J^{xy} can be transparently extracted from the rate and direction of probe spins in regions B and C precessing about an effective field due to the spins in region A [Fig. 1(a)]. By scanning a focused Raman beam across the cloud, we prepare initial states of the form $|\psi_\alpha\rangle = |\hat{\boldsymbol{\alpha}}\rangle_A |\hat{\mathbf{x}}\rangle_B |-\hat{\mathbf{x}}\rangle_C$, where $|\hat{\mathbf{u}}\rangle_R$ denotes a spin-polarized state along $\hat{\mathbf{u}}$ in region R [55]. To measure the Ising or XY couplings [Figs. 2(a) and 2(b)], we orient the spins in region A along $\hat{\boldsymbol{\alpha}} = -\hat{\mathbf{z}}$ or $\hat{\boldsymbol{\alpha}} = -\hat{\mathbf{y}}$, respectively. We prepare probe spin vectors $\boldsymbol{F}^B, \boldsymbol{F}^C$ that point in opposite directions and are approximately equal in length, such that they ideally produce no net mean field.

After initializing the desired spin texture, we switch on the drive field to induce evolution under H_{XXZ}. Representative measurements are shown in Figs. 2(a) and 2(b) for a field angle $\Theta \approx 53°$, where we expect both the Ising and XY couplings $J^{z,xy}$ to be nonzero. We extract J^z from the phase $\phi \equiv \arg[\langle f_x\rangle + i\langle f_y\rangle]$ of spins in regions B and C precessing about $\boldsymbol{\mathcal{F}}^A \propto \hat{\mathbf{z}}$ in Fig. 2(a) [55]. We extract J^{xy} analogously from measurements of the magnetization $\langle f_z\rangle = |\langle \mathbf{f}\rangle| \cos\theta$ of spins in regions B and C rotating about $\boldsymbol{\mathcal{F}}^A \propto \hat{\mathbf{y}}$ in Fig. 2(b). In each case, we compare red and blue drive detunings δ and find opposite signs of the spin rotation, indicating opposite signs of interaction [42,55]. The spatial gradient in rotation rates arises from the dependence of atom-cavity coupling $c(\zeta)$ on distance $\zeta \equiv z_c/z_R$ from cavity center [55].

The tunability of the interactions via the field angle Θ is illustrated in Fig. 2(c). For each angle, we obtain the spin-spin couplings $J^{xy,z}$ from fits to the local time evolution $\phi(t)$ or $\theta(t)$ at two positions with local couplings c, as in Figs. 2(a-b.iii). Specifically, we plot the average spin-spin coupling per intracavity photon $J^z/n = \dot{\phi}/nc\mathcal{F}_z$ (blue circles) and $J^{xy}/n = \dot{\theta}\cos\phi/nc\mathcal{F}_y$ (green squares), measured with typical intracavity photon number $n \approx 5000$. We fit the data with functional forms $J^z(\Theta) = J^z(0)\cos^2\Theta$ and $J^{xy}(\Theta) = J^{xy}(\pi/2)\sin^2\Theta$. The results are

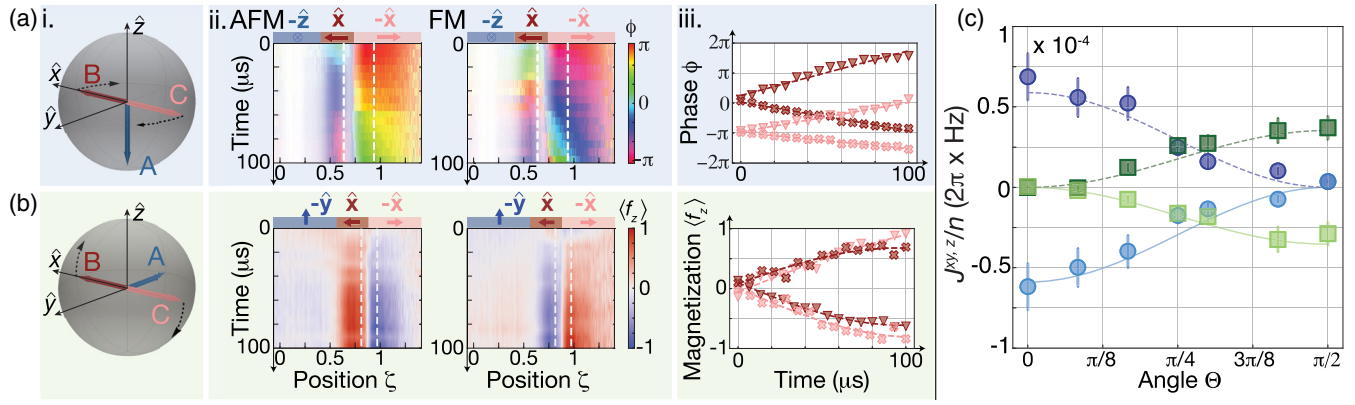

FIG. 2. Hamiltonian tomography for determining (a) Ising and (b) XY couplings. (i) Schematic of initial state and its evolution, showing probe spins precessing about mean field along (a) $-\hat{\mathbf{z}}$ or (b) $-\hat{\mathbf{y}}$. (ii) Representative measurements at $\Theta \approx 53°$ with $|\mathbf{B}| = 3$ G. The initial state is indicated above each plot, showing the direction of the spin vector in regions A, B, C. These measurements show (a) phase ϕ, with opacity indicating transverse spin length or (b) magnetization $\langle f_z \rangle$. We measure with both signs of drive detuning δ to compare antiferromagnetic (AFM) [(a) $\delta = 2\pi \times 7.5$ MHz, (b) $2\pi \times 5.5$ MHz] and ferromagnetic (FM) [(a) $\delta = -2\pi \times 5.5$ MHz, (b) $-2\pi \times 5.5$ MHz] couplings. (iii) Cuts through the regions initially polarized along $\hat{\mathbf{x}}$ (crimson) and $-\hat{\mathbf{x}}$ (pink) showing (a) $\phi(t)$ with linear fits and (b) $\langle f_z(t) \rangle$ with sinusoidal fits. Crosses (triangles) are for AFM (FM) couplings. (c) J^z (blue circles) and J^{xy} (green squares) versus Θ. Dark (light) markers are for blue (red) drive detuning $\delta = \pm 2\pi \times 5.3(4)$ MHz.

consistent with the model of the Faraday interaction, in which the couplings approach $J^z(0) = 2J^{xy}(\pi/2) = n\Omega^2/\delta$ in the large-detuning limit $|\delta| \gg \omega_Z, \kappa$ [55]. The tomography thus confirms that we have successfully engineered H_{XXZ}.

The Hamiltonian can additionally be characterized by its low-energy states and their broken symmetries. To gain intuition for the phase diagram, we first consider the case where the cavity couples to a uniformly weighted collective spin $\mathbf{F} = \sum_i \mathbf{f}_i$. The total spin F is then conserved, and the relation $|\mathbf{F}|^2 - F_z^2 = F_x^2 + F_y^2$ reveals that any accessible Hamiltonian is equivalent to an Ising model with modified $J^z_{\text{eff}} \equiv J^z - J^{xy}$. With an added transverse field $h_x\hat{\mathbf{x}}$, the system can undergo a phase transition from a paramagnet to an Ising ferromagnet with broken $\mathbb{Z}_2$ symmetry as a function of the effective Ising coupling J^z_{eff}. Remarkably, in the collective spin picture we expect the ferromagnetic Ising phase also to exist in a system with antiferromagnetic XY interactions.

To test whether this prediction extends to our system with nonuniform interactions, we generate Hamiltonians of the generic form (with $\hbar = 1$),

$$H_{\text{tot}} \approx H_{XXZ} + h_x F_x + h_z F_z, \tag{2}$$

by adding a global Raman coupling of Rabi frequency h_x and detuning h_z. Here, H_{XXZ} is the Hamiltonian of Eq. (1) with nonuniform couplings c_i, whereas the Raman coupling and detuning are approximately uniform. We prepare the paramagnetic ground state of $H_0 = h_x F_x + h_z F_z$ by adiabatically sweeping the detuning of the Raman beam from far off resonance to a final value h_z, at fixed Rabi frequency $h_x = 2\pi \times 2$ kHz. We then ramp on interactions H_{XXZ} over 5 ms to prepare a low-energy state of H_{tot} and image the resulting magnetization.

Representative images of the magnetization versus the symmetry-breaking field h_z are shown in Fig. 3(b) for different values of the Ising coupling, with $J^{xy} = 0$. In the absence of interactions ($J_z = 0$), the measured magnetization matches the prediction $\langle f_z \rangle = h_z/\sqrt{h_z^2 + h_x^2}$ [Fig. 3(b)(i)]. Antiferromagnetic Ising interactions push the spins toward the equator of the Bloch sphere [Fig. 3(b)(ii)], thereby suppressing sensitivity to changes in h_z. By contrast, ferromagnetic interactions force the spin vector toward a pole determined by the sign of h_z [Fig. 3(b)(iii)]. We summarize this behavior by plotting the magnetic susceptibility,

$$\chi \equiv \partial \cos\theta / \partial (h_z/h_x)|_{h_z=0}, \tag{3}$$

as a function of J^z in Fig. 3(c) (blue circles).

Comparing the magnetic susceptibility in the Ising model with analogous measurements for pure XY interactions [green squares in Fig. 3(c)], we observe a striking symmetry under $J^z \leftrightarrow -J^{xy}$. In both cases, the susceptibility rises sharply to the maximum value allowed by our resolution in h_z (gray line) at a critical value of the collective interaction parameter $\Lambda^{z,xy} \equiv J^{z,xy}|\mathcal{F}|$. The data are consistent with a classical model $\chi = 1/(2\Lambda^z_{\text{eff}}/h_x + 1)$, valid in the large-$\mathcal{F}$ limit, which predicts a diverging susceptibility at the critical point $-2\Lambda^z_{\text{eff}} = h_x$ of the paramagnetic-to-ferromagnetic phase transition. The model also agrees with measurements obtained by varying Λ^z_{eff} via the tuning angle Θ [Fig. 3(d)], which traces out the orange cut in the phase diagram of Fig. 3(a).

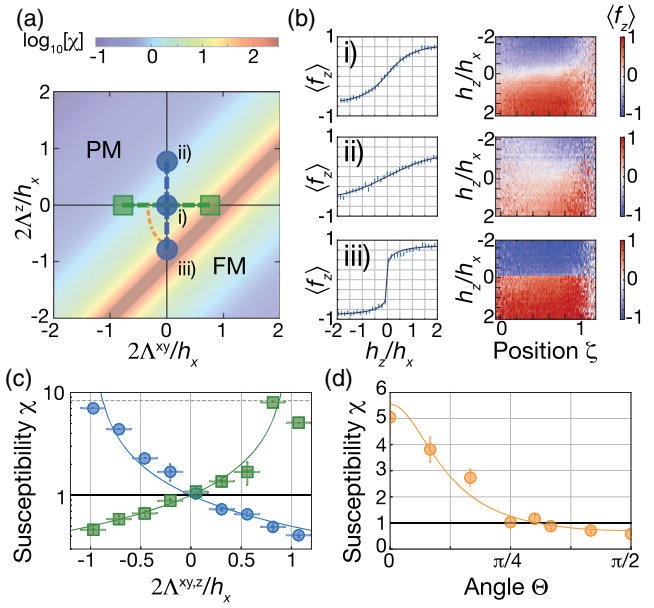

FIG. 3. Magnetic susceptibility of Ising and XY models. (a) Phase diagram of $H_{XXZ} + h_x F_x$ for collective spin model in large-$\mathcal{F}$ limit. Color shows prediction for $\log[\chi]$, which diverges at transition between paramagnetic (PM) and ferromagnetic (FM) phases. Data for (b)–(d) and corresponding theory curves were taken along blue, green, and orange cuts. (b) Representative measurements of $\langle f_z \rangle$ versus h_z at points (i)–(iii) in phase diagram; $\chi(J^z)$ is extracted from spatially averaged data (left subplots with dark blue fit curves) [55]. (c) Susceptibility χ versus J^z (blue circles) and versus J^{xy} (green squares). Dashed gray line indicates maximum detectable slope. (d) Susceptibility versus Θ at fixed drive power. For noninteracting spins, $\chi = 1$ [black lines in (c) and (d)].

Notably, the collective-spin approximation describes the magnetic susceptibility well despite spatial inhomogeneities. In addition to the variation in atom-cavity coupling $c(\zeta)$, a magnetic field gradient and inhomogeneous ac Stark shifts from the trapping lattice result in nonuniform h_z. The nonuniformity, evident in the magnetization of the noninteracting system [Fig. 3(b)(i)], is suppressed by the ferromagnetic Ising interactions [Fig. 3(b)(iii)], which tend to align the spins. However, even for antiferromagnetic interactions (both Ising and XY), the collective-spin model describes the data well, which we attribute to the spin polarization of the initial state and the aligning effect of the field h_x.

In principle, XY interactions can protect the spin coherence even without the aligning field. The XY Hamiltonian $H \propto -(\mathcal{F}_x^2 + \mathcal{F}_y^2) = \mathcal{F}_z^2 - |\boldsymbol{\mathcal{F}}|^2$ has an energy gap $\sim|\boldsymbol{\mathcal{F}}|$ between manifolds of different total spin that the analogous Ising model $H \propto \mathcal{F}_z^2$ lacks. This gap is expected to protect against dephasing from inhomogeneous fields $H_{\mathrm{inh}} = \sum_i h_{i,z} f_{i,z}$ [40]. To test this prediction, we directly compare the impact of inhomogeneous fields on systems with ferromagnetic XY and antiferromagnetic Ising interactions, which are equivalent except for the energy gap.

To probe the robustness to inhomogeneous fields, we first adiabatically prepare a low-energy state of the Hamiltonian $H_{\mathrm{tot}} = H_{XXZ} + h_x F_x + H_{\mathrm{inh}}$, where H_{inh} consists of $\hat{\mathbf{z}}$ fields $h_{i,z} \lesssim h_x$. We then quench off the aligning field h_x and image the subsequent dynamics. To calibrate the inhomogeneous field H_{inh}, we first perform this quench without interactions and image the dephasing of the spins, as shown in Fig. 4(a) for tuning angle $\Theta = \pi/2$. We plot the total phase winding $\phi_L(t)$ across a length $L = 1$ mm for $\Theta = \pi/2$ (green dashed line) and $\Theta = 0$ (blue dashed line) in Fig. 4(c). For both angles, we observe similar magnitudes of the gradient $\mu = L^{-1} d\phi_L/dt$, as well as a small but nonzero initial phase winding $\phi_L(0)$ due to finite strength of the aligning field h_x before the quench. Whereas introducing Ising interactions has no effect on the dephasing (blue circles), XY interactions completely suppress the growth of phase winding (green squares).

The onset of protected spin coherence is summarized in Fig. 4(d), where we plot the global contrast $C_g \equiv (1/N)\sqrt{F_x^2 + F_y^2}$ versus interaction strength. We find an increase in contrast, indicating phasing of the spins, when the XY interaction strength becomes comparable to the gradient across the cloud, i.e., $\Lambda^{xy} \sim \mu \mathrm{L}$. This condition can be understood in a mean-field picture by noting that the interactions produce an effective transverse field $\Lambda^{xy}\hat{\mathbf{x}}$, which must overcome the dephasing influence of differential $\hat{\mathbf{z}}$ fields of order μL [55]. Equivalently, in a quantum mechanical description, interactions can protect against variations in h_z that are small compared with the energy cost to flip a single spin, set by the gap of order Λ^{xy} between sectors of different total spin [55].

Our intuitive understanding of the gap protection is confirmed by numerical simulations of the mean-field dynamics. Both the data and simulations [solid curves in Fig. 4(d)] show the contrast increasing to a value $C_g \approx 0.6$, limited primarily by imperfect coherence $C_0 = 0.67(5)$ of the initial state. A smaller effect included in the solid curves is spontaneous emission. Comparing with an idealized model without spontaneous emission (dotted curves) shows that the interactions enhance coherence with minimal detriment from free-space scattering, thanks to the strong collective atom-light coupling.

In future work, spin-exchange interactions can be applied to maximize coherence in light-induced spin squeezing protocols [31–33,48,57,58], operating either adiabatically or via one-axis twisting dynamics [36,40]. Notably, during one-axis twisting, the emergent many-body gap can protect the spin length without producing any additional dynamics, in contrast to an aligning transverse field that would cause unwanted rotations. Gap protection could suppress even time-varying inhomogeneities arising from atomic motion, a benefit over spin echo pulses [59]. Extended to other platforms, gap protection can aid in

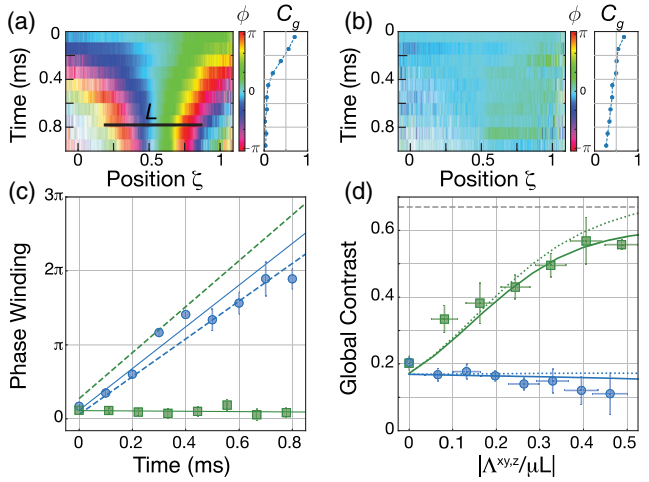

FIG. 4. Protection against dephasing. (a),(b) Phase ϕ and global contrast C_g at $\Theta = \pi/2$ for (a) no interactions and (b) XY interactions $[\Lambda^{xy}/\mu L = -0.43(4)]$, in magnetic field gradient $|\mu| = 2\pi \times 2.1(1)$ kHz/z_R. Opacity indicates length of transverse spin component. (c) Phase winding $\phi_L(t)$ for ferromagnetic XY interactions (squares, $\Theta = \pi/2$) or antiferromagnetic Ising interactions (circles, $\Theta = 0$) of equal strength. Dashed lines show ϕ_L in noninteracting systems at $\Theta = 0$ (blue) and $\Theta = \pi/2$ (green). (d) Global contrast C_g versus collective interaction strength $|\Lambda^{xy,z}|$ for XY (green squares) and Ising (blue circles) interactions, at $t = 0.5$ ms. Solid (dotted) curves show mean-field model with (without) free-space scattering. Dashed gray line indicates initial contrast C_0.

preserving global spin coherence while using local (e.g., dipolar) interactions for entanglement generation [60–66].

Much territory remains for further exploration of the nonlocal XXZ model. Perturbations of the antiferromagnetic Heisenberg model may yield chiral or valance-bond ground states [67], and the spin-1 structure may enrich the phase diagram [38,42,68,69]. Adiabatic ramps could be used to prepare low-energy states of Ising models encoding combinatorial optimization problems [27]. Modifying the interaction graph by Floquet driving [14] or local addressing can enable fast scrambling [18–20,23] or simulations of spin glasses [15–17].

This work was supported by the DOE Office of Science, Office of High Energy Physics and Office of Basic Energy Sciences under Grant No. DE-SC0019174. A. P. and E. S. C. acknowledge support from the NSF under Grant No. PHY-1753021. We additionally acknowledge support from the NSF Graduate Research Fellowship Program (E. J. D. and E. S. C.), from the Hertz Foundation (E. J. D.), and from the National Defense Science and Engineering Graduate Fellowship (A. P.).

E. J. D., A. P., and E. S. C. contributed equally to this work.

[1] P. W. Anderson, Mater. Res. Bull. **8**, 153 (1973).
[2] A. Kitaev, Ann. Phys. (Amsterdam) **321**, 2 (2006).
[3] L.-M. Duan, E. Demler, and M. D. Lukin, Phys. Rev. Lett. **91**, 090402 (2003).
[4] R. Barnett, D. Petrov, M. Lukin, and E. Demler, Phys. Rev. Lett. **96**, 190401 (2006).
[5] S. Trotzky, P. Cheinet, S. Fölling, M. Feld, U. Schnorrberger, A. M. Rey, A. Polkovnikov, E. A. Demler, M. D. Lukin, and I. Bloch, Science **319**, 295 (2008).
[6] J. Simon, W. S. Bakr, R. Ma, M. E. Tai, P. M. Preiss, and M. Greiner, Nature (London) **472**, 307 (2011).
[7] A. Browaeys and T. Lahaye, Nat. Phys. **16**, 132 (2020).
[8] H. Bernien, S. Schwartz, A. Keesling, H. Levine, A. Omran, H. Pichler, S. Choi, A. S. Zibrov, M. Endres, M. Greiner *et al.*, Nature (London) **551**, 579 (2017).
[9] J. Zeiher, J.-Y. Choi, A. Rubio-Abadal, T. Pohl, R. van Bijnen, I. Bloch, and C. Gross, Phys. Rev. X **7**, 041063 (2017).
[10] E. Guardado-Sanchez, P. T. Brown, D. Mitra, T. Devakul, D. A. Huse, P. Schauß, and W. S. Bakr, Phys. Rev. X **8**, 021069 (2018).
[11] A. Micheli, G. Brennen, and P. Zoller, Nat. Phys. **2**, 341 (2006).
[12] A. W. Glaetzle, M. Dalmonte, R. Nath, C. Gross, I. Bloch, and P. Zoller, Phys. Rev. Lett. **114**, 173002 (2015).
[13] N. Y. Yao, M. P. Zaletel, D. M. Stamper-Kurn, and A. Vishwanath, Nat. Phys. **14**, 405 (2018).
[14] C.-L. Hung, A. González-Tudela, J. I. Cirac, and H. Kimble, Proc. Natl. Acad. Sci. U.S.A. **113**, E4946 (2016).
[15] P. Strack and S. Sachdev, Phys. Rev. Lett. **107**, 277202 (2011).
[16] S. Gopalakrishnan, B. L. Lev, and P. M. Goldbart, Phys. Rev. Lett. **107**, 277201 (2011).
[17] M. Buchhold, P. Strack, S. Sachdev, and S. Diehl, Phys. Rev. A **87**, 063622 (2013).
[18] B. Swingle, G. Bentsen, M. Schleier-Smith, and P. Hayden, Phys. Rev. A **94**, 040302(R) (2016).
[19] G. Bentsen, T. Hashizume, A. S. Buyskikh, E. J. Davis, A. J. Daley, S. S. Gubser, and M. Schleier-Smith, Phys. Rev. Lett. **123**, 130601 (2019).
[20] J. Marino and A. M. Rey, Phys. Rev. A **99**, 051803(R) (2019).
[21] F. Mivehvar, H. Ritsch, and F. Piazza, Phys. Rev. Lett. **122**, 113603 (2019).
[22] G. Bentsen, I.-D. Potirniche, V. B. Bulchandani, T. Scaffidi, X. Cao, X.-L. Qi, M. Schleier-Smith, and E. Altman, Phys. Rev. X **9**, 041011 (2019).
[23] J. Kim, X. Cao, and E. Altman, Phys. Rev. B **101**, 125112 (2020).
[24] N. Defenu, T. Enss, M. Kastner, and G. Morigi, Phys. Rev. Lett. **121**, 240403 (2018).
[25] E. Colella, R. Citro, M. Barsanti, D. Rossini, and M.-L. Chiofalo, Phys. Rev. B **97**, 134502 (2018).
[26] M. W. Johnson, M. H. Amin, S. Gildert, T. Lanting, F. Hamze, N. Dickson, R. Harris, A. J. Berkley, J. Johansson, P. Bunyk *et al.*, Nature (London) **473**, 194 (2011).
[27] A. Lucas, Front. Phys. **2**, 5 (2014).
[28] S. Morrison and A. S. Parkins, Phys. Rev. Lett. **100**, 040403 (2008).

[29] E. I. R. Chiacchio and A. Nunnenkamp, Phys. Rev. Lett. **122**, 193605 (2019).
[30] J. A. Muniz, D. Barberena, R. J. Lewis-Swan, D. J. Young, J. R. Cline, A. M. Rey, and J. K. Thompson, Nature **580**, 602 (2020)..
[31] I. D. Leroux, M. H. Schleier-Smith, and V. Vuletić, Phys. Rev. Lett. **104**, 073602 (2010).
[32] O. Hosten, R. Krishnakumar, N. J. Engelsen, and M. A. Kasevich, Science **352**, 1552 (2016).
[33] B. Braverman, A. Kawasaki, E. Pedrozo-Peñafiel, S. Colombo, C. Shu, Z. Li, E. Mendez, M. Yamoah, L. Salvi, D. Akamatsu *et al.*, Phys. Rev. Lett. **122**, 223203 (2019).
[34] G. Barontini, L. Hohmann, F. Haas, J. Estève, and J. Reichel, Science **349**, 1317 (2015).
[35] E. Davis, G. Bentsen, and M. Schleier-Smith, Phys. Rev. Lett. **116**, 053601 (2016).
[36] J. Hu, W. Chen, Z. Vendeiro, A. Urvoy, B. Braverman, and V. Vuletić, Phys. Rev. A **96**, 050301(R) (2017).
[37] R. J. Lewis-Swan, M. A. Norcia, J. R. K. Cline, J. K. Thompson, and A. M. Rey, Phys. Rev. Lett. **121**, 070403 (2018).
[38] S. J. Masson, M. D. Barrett, and S. Parkins, Phys. Rev. Lett. **119**, 213601 (2017).
[39] V. D. Vaidya, Y. Guo, R. M. Kroeze, K. E. Ballantine, A. J. Kollár, J. Keeling, and B. L. Lev, Phys. Rev. X **8**, 011002 (2018).
[40] M. A. Norcia, R. J. Lewis-Swan, J. R. Cline, B. Zhu, A. M. Rey, and J. K. Thompson, Science **361**, 259 (2018).
[41] M. Landini, N. Dogra, K. Kröger, L. Hruby, T. Donner, and T. Esslinger, Phys. Rev. Lett. **120**, 223602 (2018).
[42] E. J. Davis, G. Bentsen, L. Homeier, T. Li, and M. H. Schleier-Smith, Phys. Rev. Lett. **122**, 010405 (2019).
[43] N. Spethmann, J. Kohler, S. Schreppler, L. Buchmann, and D. M. Stamper-Kurn, Nat. Phys. **12**, 27 (2016).
[44] C. Georges, J. G. Cosme, L. Mathey, and A. Hemmerich, Phys. Rev. Lett. **121**, 220405 (2018).
[45] A. Kuzmich and T. A. B. Kennedy, Phys. Rev. Lett. **92**, 030407 (2004).
[46] J. Hu, W. Chen, Z. Vendeiro, H. Zhang, and V. Vuletić, Phys. Rev. A **92**, 063816 (2015).
[47] L. Dellantonio, S. Das, J. Appel, and A. S. Sørensen, Phys. Rev. A **95**, 040301(R) (2017).
[48] Y. Wu, R. Krishnakumar, J. Martínez-Rincón, B. K. Malia, O. Hosten, and M. A. Kasevich, arXiv:1912.08334 [Phys. Rev. A (to be published)].
[49] C. Deutsch, F. Ramirez-Martinez, C. Lacroûte, F. Reinhard, T. Schneider, J.-N. Fuchs, F. Piéchon, F. Laloë, J. Reichel, and P. Rosenbusch, Phys. Rev. Lett. **105**, 020401 (2010).
[50] G. K. Büning, J. Will, W. Ertmer, E. Rasel, J. Arlt, C. Klempt, F. Ramirez-Martinez, F. Piéchon, and P. Rosenbusch, Phys. Rev. Lett. **106**, 240801 (2011).
[51] S. Choi, J. Choi, R. Landig, G. Kucsko, H. Zhou, J. Isoya, F. Jelezko, S. Onoda, H. Sumiya, V. Khemani *et al.*, Nature (London) **543**, 221 (2017).
[52] J. Zhang, P. Hess, A. Kyprianidis, P. Becker, A. Lee, J. Smith, G. Pagano, I.-D. Potirniche, A. C. Potter, A. Vishwanath *et al.*, Nature (London) **543**, 217 (2017).
[53] K. Hammerer, A. S. Sørensen, and E. S. Polzik, Rev. Mod. Phys. **82**, 1041 (2010).
[54] J. Kohler, N. Spethmann, S. Schreppler, and D. M. Stamper-Kurn, Phys. Rev. Lett. **118**, 063604 (2017).
[55] See Supplemental Material at http://link.aps.org/supplemental/10.1103/PhysRevLett.125.060402, which includes Ref. [56], for supporting derivations.
[56] H. Tanji-Suzuki, I. D. Leroux, M. H. Schleier-Smith, M. Cetina, A. T. Grier, J. Simon, and V. Vuletić, in *Advances in Atomic, Molecular, and Optical Physics* (Elsevier, 2011), Vol. 60, pp. 201–237.
[57] J. G. Bohnet, K. C. Cox, M. A. Norcia, J. M. Weiner, Z. Chen, and J. K. Thompson, Nat. Photonics **8**, 731 (2014).
[58] O. Hosten, N. J. Engelsen, R. Krishnakumar, and M. A. Kasevich, Nature (London) **529**, 505 (2016).
[59] M. H. Schleier-Smith, I. D. Leroux, and V. Vuletić, Phys. Rev. Lett. **104**, 073604 (2010).
[60] A. M. Rey, L. Jiang, M. Fleischhauer, E. Demler, and M. D. Lukin, Phys. Rev. A **77**, 052305 (2008).
[61] P. Cappellaro and M. D. Lukin, Phys. Rev. A **80**, 032311 (2009).
[62] M. S. Rudner, L. M. K. Vandersypen, V. Vuletić, and L. S. Levitov, Phys. Rev. Lett. **107**, 206806 (2011).
[63] I. Bouchoule and K. Mølmer, Phys. Rev. A **65**, 041803(R) (2002).
[64] L. I. R. Gil, R. Mukherjee, E. M. Bridge, M. P. A. Jones, and T. Pohl, Phys. Rev. Lett. **112**, 103601 (2014).
[65] R. Kaubruegger, P. Silvi, C. Kokail, R. van Bijnen, A. M. Rey, J. Ye, A. M. Kaufman, and P. Zoller, Phys. Rev. Lett. **123**, 260505 (2019).
[66] V. Borish, O. Marković, J. A. Hines, S. V. Rajagopal, and M. Schleier-Smith, Phys. Rev. Lett. **124**, 063601 (2020).
[67] C. Mudry and E. Fradkin, Phys. Rev. B **40**, 11177 (1989).
[68] X.-Y. Luo, Y.-Q. Zou, L.-N. Wu, Q. Liu, M.-F. Han, M. K. Tey, and L. You, Science **355**, 620 (2017).
[69] Z. Zhiqiang, C. H. Lee, R. Kumar, K. Arnold, S. J. Masson, A. Parkins, and M. Barrett, Optica **4**, 424 (2017).